

# Optimal Attenuation of Known Periodic Disturbances: a Convex Control Design Approach

**Goele Pipeleers, Bram Demeulenaere, Joris De Schutter, Jan Swevers**

K.U.Leuven, Department of Mechanical Engineering,  
Celestijnenlaan 300 B, B-3001, Heverlee, Belgium  
e-mail: [goele.pipeleers@mech.kuleuven.be](mailto:goele.pipeleers@mech.kuleuven.be)

## Abstract

This paper discusses the design of optimal linear controllers for the attenuation of known periodic disturbances in linear systems. A general framework is developed allowing for a variety of control configurations, robustness and performance specifications, and input constraints. The optimal control design is formulated as a convex optimization problem. To robustify the framework for uncertainty on the disturbance period, two strategies are proposed and compared to each other for a numerical example: (i) a worst-case strategy and (ii) a sensitivity-based approach.

## 1 INTRODUCTION

Regulation of the plant output in the presence of disturbances is a relevant control problem with many practical applications, for example the design of active vibration isolators for sensitive equipment or the stabilization of civil structures during earthquakes. Often, the dominant disturbance is known, for instance a periodic disturbance with a (roughly) known frequency content, such as disturbances originating from nearby combustion engines or rotating unbalances; or an impact disturbance, such as structureborn impact noise of punching machines [4]. A controller design that accounts for the characteristics of the dominant disturbance is most likely to yield a better performance compared to a general regulator design.

Based on the theory of Boyd and Barratt [1], a general framework is developed here to design optimal regulators for periodic disturbances with known frequency content. Since in many applications the period of the disturbance is only roughly known or subject to small variations, the framework is robustified for uncertainty on the disturbance period. For this purpose, two strategies are proposed in this paper and compared to each other for a numerical simulation example.

The key feature of the framework is the formulation of the optimal controller design as a convex optimization problem. Convex optimization problems are nonlinear optimization problems that have the unique property that all local optima are also globally optimal. As a result, it is guaranteed that the global optimum be found, with great speed and without requiring an initial guess. Moreover, trade-off curves of competing performance specifications are readily obtained for convex optimization problems, as explained in [2].

The framework is elaborated here for the design of a discrete single-input single-output (SISO) feedback controller for a stable plant. However, it also applies to other control problems. Adaptations needed for unstable plants are indicated in the text. The extension for multiple-input multiple-output (MIMO) control and feedforward control is straightforward.

The following nomenclature is used: The sampling time and frequency are denoted by  $T_s$  and  $f_s$ , respectively. Time instants are indicated by  $t_k = kT_s$ , and sampled signals by  $x(k) = x(t_k)$ . Discrete transfer functions (TF) are denoted by  $X(z)$ , and the corresponding frequency response function (FRF) by  $X(\omega)$  (instead of  $X(e^{j\omega T_s})$ ). Vectors and matrices are represented by bold characters, e.g., transfer matrix  $\mathbf{X}(z)$ .

Section 2 details the methodology of the framework for the design of a SISO feedback controller. Thereafter the properties of the obtained controllers are illustrated for a simulation example (Section 3). Finally, the main conclusions are summarized in Section 4.

## 2 Methodology

This section is organized as follows: Section 2.1 introduces the SISO control configuration for which the framework is developed. In the framework, the optimal control problem is translated into a numerical optimization problem. Section 2.2 elaborates on the essential constraints, such as stability and realizability. Section 2.3 details the implementation of the performance specifications and input constraints. The resulting optimization problem and its computational aspects are discussed in 2.4. Section 2.5 proposes two strategies to improve the robustness of the solution for uncertainty on the disturbance period.

### 2.1 Control Setup

Figure 1 shows the block diagram of the SISO feedback control system. The dominant disturbance  $d(k)$  is periodic with period  $T_0$  ( $f_0 = 1/T_0$ ,  $\omega_0 = 2\pi f_0$ ):

$$d(k) = \sum_{m=-M}^M D_m \exp(jm\omega_0 kT_s), \quad (1)$$

and its frequency content (i.e.,  $D_m, \forall m$ ) is known.  $m : \{1, \dots, M\}$  indicates the harmonics of  $d(k)$ , and  $M$  the highest harmonic. Besides the periodic disturbance  $d(k)$ , also sensor noise  $n_s(k)$  and input referred process noise  $n_p(k)$ , both stochastic signals, are considered.  $x(k)$  is the plant output to be regulated,  $u(k)$  the control signal, and  $y(k)$  the sensed output.  $G(z)$  is the TF of the plant model, and  $G_d(z)$  the TF of the disturbance model. Both models are assumed to be stable. The controller  $C(z)$  is designed so as to minimize the response  $x(k)$  to both the periodic ( $d(k)$ ) and the stochastic ( $n_p(k), n_s(k)$ ) disturbances.

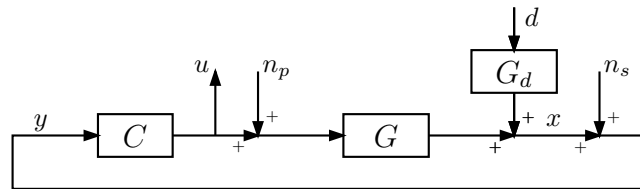


Figure 1: Block diagram of a SISO feedback control system.

The control configuration of Fig. 1 is converted into the general control configuration of Fig. 2 where the exogenous input  $w(k)$ , the exogenous output  $z(k)$  and the generalized plant  $P(z)$  are given by

$$w(k) = [d(k) \quad n_p(k) \quad n_s(k)]^T; \quad (2)$$

$$z(k) = [x(k) \quad y(k) \quad u(k)]^T; \quad (3)$$

$$P(z) = \left[ \begin{array}{ccc|c} G_d(z) & G(z) & 0 & G(z) \\ G_d(z) & G(z) & 1 & G(z) \\ 0 & 0 & 0 & 1 \\ \hline G_d(z) & G(z) & 1 & G(z) \end{array} \right]; \quad (4)$$

$$= \left[ \begin{array}{c|c} P_{11}(z) & P_{12}(z) \\ \hline P_{21}(z) & P_{22}(z) \end{array} \right]. \quad (5)$$

The closed-loop transfer matrix is denoted by  $\mathbf{H}(z)$ :

$$\mathbf{z}(k) = \mathbf{H}(z)\mathbf{w}(k), \quad (6)$$

$$\mathbf{H}(z) = \begin{bmatrix} H_{11}(z) & H_{12}(z) & H_{13}(z) \\ H_{21}(z) & H_{22}(z) & H_{23}(z) \\ H_{31}(z) & H_{32}(z) & H_{33}(z) \end{bmatrix}. \quad (7)$$

By including  $n_s(k)$  and  $n_p(k)$  in  $\mathbf{w}(z)$ , and  $y(k)$  and  $u(k)$  in  $\mathbf{z}(k)$ , the closed loop is internally stable whenever  $\mathbf{H}(z)$  is stable [1].

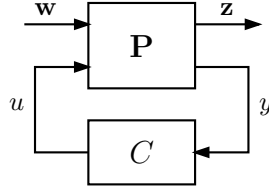


Figure 2: General control configuration.

## 2.2 Internal stability and realizability of $\mathbf{H}(z)$

Boyd and Barratt [1] have shown that many performance and robustness specifications are convex functions if formulated in the closed-loop transfer matrix  $\mathbf{H}(z)$ . In order to obtain a convex optimization problem, the optimal control problem is therefore formulated as an optimization problem in  $\mathbf{H}(z)$ . The corresponding controller  $C(z)$  is calculated afterwards. Essential constraints on  $\mathbf{H}(z)$  are: (i) the closed-loop system should be internally stable, and (ii)  $\mathbf{H}(z)$  results from the interconnection of the generalized plant  $\mathbf{P}(z)$  and a controller  $C(z)$ . The latter constraint imposes the so-called realizability of  $\mathbf{H}(z)$  and guarantees that the corresponding controller can be computed.

### 2.2.1 Parameterization of $\mathbf{H}(z)$

Boyd and Barratt [1] have shown that the set  $\mathcal{H}$  of stable, realizable closed-loop transfer matrices is given by the parameterization

$$\mathcal{H} = \{\mathbf{H}(z) = \mathbf{T}_1(z) + \mathbf{T}_2(z)Q(z)\mathbf{T}_3(z) \mid Q(z) \text{ stable}\} . \quad (8)$$

Transfer matrices  $\mathbf{T}_1(z)$ ,  $\mathbf{T}_2(z)$  and  $\mathbf{T}_3(z)$  are determined by the plant. Transfer function  $Q(z)$  is called the free parameter of  $\mathbf{H}(z)$  and must be stable. In the case of a stable plant,  $\mathbf{T}_1(z)$ ,  $\mathbf{T}_2(z)$  and  $\mathbf{T}_3(z)$  equal  $\mathbf{P}_{11}(z)$ ,  $\mathbf{P}_{12}(z)$  and  $\mathbf{P}_{21}(z)$ , respectively. For unstable plants, representation (8) is also valid but more cumbersome expressions for  $\mathbf{T}_1(z)$ ,  $\mathbf{T}_2(z)$  and  $\mathbf{T}_3(z)$  result [1].

By including (8) in the optimization problem both the stability and the realizability of  $\mathbf{H}(z)$  are guaranteed. The stability of  $\mathbf{H}(z)$  implies closed loop internal stability, since  $n_s(k)$  and  $n_p(k)$  are included in  $\mathbf{w}(z)$ , and  $y(k)$  and  $u(k)$  in  $\mathbf{z}(k)$ , as mentioned earlier.

The corresponding controller  $C(z)$  is calculated from  $Q(z)$  and the plant  $\mathbf{P}(z)$ . For the control problem of Section 2.1,  $C(z)$  is given by

$$C(z) = \frac{Q(z)}{1 + P_{22}(z)Q(z)}. \quad (9)$$

### 2.2.2 Model Structure of $Q(z)$

In choosing a model structure for  $Q(z)$  two requirements are essential in order to obtain a convex optimization problem. First,  $Q(z)$  must depend affinely on its model parameters. Equation (8) shows  $\mathbf{H}(z)$  to depend affinely on  $Q(z)$  and therefore convex functions of  $\mathbf{H}(z)$  are also convex when formulated in terms of  $Q(z)$  [2]. By using a model structure that relates  $Q(z)$  affinely to its model parameters, the convexity of functions of  $\mathbf{H}(z)$  is preserved when formulated in the model parameters of  $Q$ . Second, the stability of  $Q(z)$  must not require nonconvex constraints on its model parameters.

In this paper a finite-impulse-response (FIR) model of length  $L$  is proposed as the model structure for  $Q(z)$ :

$$Q(z) = \sum_{l=0}^{L-1} q_l z^{-l} . \quad (10)$$

This model structure fulfills both of the aforementioned requirements, since (i)  $Q(z)$  depends affinely on the model parameters  $q_l$ , and (ii) actually no constraints are required to impose stability of  $Q(z)$ , since (10) is stable  $\forall q_l \in \mathbb{R}$ .

## 2.3 Performance Specifications and Input Constraints

For an overview of the performance specifications and input constraints that result in a convex optimization problem, the reader is referred to [1]. For the optimal attenuation of periodic disturbances, the following performance specifications and input constraints are relevant:

### 2.3.1 Performance Specifications

The controller design aims at reducing the response  $x(k)$  as much as possible. Both components of  $x(k)$ , i.e., the periodic and the stochastic component, are considered:

- periodic component:  $f_1$ , the mean square of the periodic component of  $x(k)$  quantifies the response to  $d(k)$ .  $f_1$  is calculated from the harmonic components  $X_m$  of this periodic response:

$$f_1 = 2 \sum_{m=1}^M |X_m|^2 , \quad (11)$$

where

$$X_m = H_{11}(m\omega_0)D_m , \quad \forall m: 1, \dots, M . \quad (12)$$

- stochastic component: The influence of the process noise  $n_p(k)$  on  $x(k)$  is quantified by  $f_2$ , the weighted  $H_\infty$ -norm of  $H_{12}$ :

$$f_2 = M_{12} , \quad (13)$$

where  $M_{12}$  satisfies

$$\left| \frac{H_{12}(\omega)}{W_{12}(\omega)} \right| \leq M_{12} , \quad \forall \omega \in [0, \pi f_s] . \quad (14)$$

Similarly, the influence of the sensor noise  $n_s(k)$  on  $x(k)$  is quantified by  $f_3$ , the weighted  $H_\infty$ -norm of  $H_{13}$ :

$$f_3 = M_{13} , \quad (15)$$

where  $M_{13}$  satisfies

$$\left| \frac{H_{13}(\omega)}{W_{13}(\omega)} \right| \leq M_{13} , \quad \forall \omega \in [0, \pi f_s] . \quad (16)$$

Weighting functions  $W_{12}(\omega)$  and  $W_{13}(\omega)$  are real-valued functions, chosen by the control engineer.

### 2.3.2 Input Constraints

In order to obtain a realistic actuator signal, bound and rate constraints on the periodic component  $u_p(k)$  of  $u(k)$  are imposed:

$$|u_p(k)| \leq u_{\max}, \quad \forall k \in \mathbb{N}; \quad (17)$$

$$|u_p(k+1) - u_p(k)| \leq \dot{u}_{\max}, \quad \forall k \in \mathbb{N}. \quad (18)$$

$u_p(k)$  is the closed-loop response to  $d(k)$  and therefore given by

$$u_p(k) = \sum_{m=-M}^M U_m \exp(jm\omega_0 k T_s), \quad \forall k : 1, \dots, N_d; \quad (19)$$

$$U_m = H_{31}(m\omega_0) D_m, \quad \forall m : 1, \dots, M. \quad (20)$$

### 2.3.3 Discretization

Goal functions  $f_2$  (13) and  $f_3$  (15) require the evaluation of constraints (14,16) on the interval  $[0, \pi f_s]$ , resulting in an infinite dimensional optimization problem. To reduce this optimization problem to a finite dimensional problem, a finite number  $N$  of time instants are considered. This corresponds to a discretization of the frequency axis:  $\delta f = f_s/N$ ,  $\delta\omega = 2\pi\delta f$ .  $N$  has to be chosen such that the time window  $NT_s$  corresponds to an integer number of periods of  $d(k)$ .

## 2.4 Numerical Optimization Problem

For reasons of computational efficiency, the second-order cone constraints (14,16) are approximated by:

$$|\Re(H_{12}(\omega))| + |\Im(H_{12}(\omega))| \leq M_{12}W_{12}(\omega); \quad (21)$$

$$|\Re(H_{13}(\omega))| + |\Im(H_{13}(\omega))| \leq M_{13}W_{13}(\omega). \quad (22)$$

These constraints can be transformed into a set of linear inequality constraints [2]. Without this approximation, the optimization problem is a second-order cone program (SOCP) and hence convex. The approximation reduces the SOCP to a convex quadratic program (QP). For QPs very reliable and efficient solvers exist, like MINOS [3], used here.

Compared to (14,16), constraints (21,22) are conservative. The results of Section 3.3 however show that for the simulation example of Section 3.1 this conservatism is limited.

The structure of the resulting optimization problem is described below. The following subscripts are used:  $n : \{0, \dots, N/2\}$  indicates the frequency lines,  $k : \{0, \dots, N-1\}$  the time samples,  $m : \{1, \dots, M\}$  the harmonics of  $d(k)$ , and  $l : \{0, \dots, L-1\}$  the parameters  $q_l$  of the FIR-model of  $Q(z)$ .

**Variables:** the real and imaginary part of the complex variables  $\mathbf{H}(n\delta\omega)$ ,  $Q(n\delta\omega)$ ,  $X_m$  and  $U_m$ ; and the real variables  $q_l$  and  $u_p(k)$ .

**Constraints:**

$$\mathbf{H}(n\delta\omega) = \mathbf{T}_1(n\delta\omega) + \mathbf{T}_2(n\delta\omega)Q(n\delta\omega)\mathbf{T}_3(n\delta\omega) ; \quad (23)$$

$$Q(n\delta\omega) = \sum_{l=0}^{L-1} q_l \exp(-jn\delta\omega l T_s) ; \quad (24)$$

$$X_m = H_{11}(m\omega_0) D_m ; \quad (25)$$

$$U_m = H_{31}(m\omega_0) D_m ; \quad (26)$$

$$u_p(k) = \sum_{m=-M}^M U_m \exp(jm\omega_0 k T_s) ; \quad (27)$$

$$|\Re(H_{12}(n\delta\omega))| + |\Im(H_{12}(n\delta\omega))| \leq M_{12}W_{12}(n\delta\omega) ; \quad (28)$$

$$|\Re(H_{13}(n\delta\omega))| + |\Im(H_{13}(n\delta\omega))| \leq M_{13}W_{13}(n\delta\omega) ; \quad (29)$$

$$|u_p(k)| \leq u_{\max} ; \quad (30)$$

$$|u_p(k+1) - u_p(k)| \leq \dot{u}_{\max} . \quad (31)$$

**Goal Function:** In order to take both  $f_1$ ,  $f_2$  and  $f_3$  into account, a weighted sum of these three goal functions is used:

$$f = f_1 + \alpha_2 f_2 + \alpha_3 f_3 . \quad (32)$$

Because the optimization problem is convex, the trade-off surface for these three goal functions can be readily computed by varying  $\alpha_2$  and  $\alpha_3$  in (32) and solving the corresponding optimization problem [2]. Moreover the convexity guarantees that for each optimization problem instance the global optimum is found with great speed.

## 2.5 Robust Implementation for Uncertainty on $\omega_0$

In many applications the period  $T_0$  of the disturbance is only roughly known or subject to small variations. Therefore special attention is paid to the robustness of the results with respect to uncertainty on  $\omega_0$ . Two strategies are adopted to increase the robustness under this uncertainty. This subsection describes these strategies, together with the adaptations needed to the above described non-robust optimization problem.

### 2.5.1 Worst-Case Goal Function

This implementation assumes the upper and lower bound of  $\omega_0$  to be known:  $\omega_0 \in [\omega_L, \omega_U]$ . In this interval a finite number of values for  $\omega_0$  are considered, namely, those coinciding with a discrete frequency line:

$$\{\omega_0^i\} = \{\omega_0 \in [\omega_L, \omega_U] \mid \exists n \in \mathbb{N} : \omega_0 = n\delta\omega\} . \quad (33)$$

Goal function  $f_1$  (11) is replaced by its worst-case value for  $\omega_0 \in \{\omega_0^i\}$ :

$$f_{1,wc} = M_{f_1} , \quad (34)$$

where

$$f_1^i = 2 \sum_{m=1}^M |X_m^i|^2 \leq M_{f_1} , \quad \forall i , \quad (35)$$

$$X_m^i = H_{11}(m\omega_0^i) D_m , \quad \forall m , \quad \forall i . \quad (36)$$

Adding convex quadratic constraints (35) to the optimization problem results in a convex quadratically constrained quadratic program, instead of a QP.

## 2.5.2 Sensitivity-Based Approach

Robustness of the solution for uncertainty on  $\omega_0$  requires that the mean square value of  $x(k)$  does not vary too much whenever  $\omega_0$  varies, or equivalently, that  $|H_{11}(\omega)|$  may not vary too much around  $m\omega_0$ ,  $m : 1, \dots, M$ . The variation of  $|H_{11}(\omega)|$  can be limited by enforcing the first and higher order derivatives of  $|H_{11}(\omega)|$  to be zero at  $m\omega_0$ . In this paper, only the first and second order derivatives are constrained:

$$\left. \frac{d|H_{11}(\omega)|}{d\omega} \right|_{m\omega_0} = \left. \frac{d^2|H_{11}(\omega)|}{d\omega^2} \right|_{m\omega_0} = 0, \forall m. \quad (37)$$

Since these constraints are not convex, they are replaced by

$$\left. \frac{d\Re(H_{11}(\omega))}{d\omega} \right|_{m\omega_0} = \left. \frac{d^2\Re(H_{11}(\omega))}{d\omega^2} \right|_{m\omega_0} = 0; \quad (38)$$

$$\left. \frac{d\Im(H_{11}(\omega))}{d\omega} \right|_{m\omega_0} = \left. \frac{d^2\Im(H_{11}(\omega))}{d\omega^2} \right|_{m\omega_0} = 0. \quad (39)$$

This approximation is only little conservative whenever both  $\Re(H_{11}(m\omega_0))$  and  $\Im(H_{11}(m\omega_0))$  are small, which may be expected since this is the goal of the controller design.

Constraints (38,39) constitute a set of  $4M$  linear equality constraints in the FIR parameters  $q_l$  of  $Q(z)$ <sup>1</sup>. Consequently, by adding these constraints to the optimization problem, it remains a QP.

Compared to the worst-case strategy, this sensitivity-based approach does not start from an uncertainty interval for which robustness is guaranteed. It is a local strategy in the sense that the constraints only enforce  $|H_{11}(\omega)|$  to be constant near the nominal value of  $\omega_0$ , but nothing is known about the interval of  $\omega_0$  for which this approach yields good performance.

## 3 Numerical Results

This section illustrates the framework for the simulation example introduced in Section 3.1. Section 3.2 discusses the trade-off between  $f_1$  (11) and  $f_3$  (15) for both the non-robust and the robust implementations. For certain points of these trade-off curves, the corresponding closed-loop system is discussed in detail in Section 3.3.

### 3.1 Simulation Example

To illustrate the framework, it is used to design a regulator for the system shown in Fig. 3. The mass  $m = 0.5$  kg is supported by an active suspension system composed of a spring (spring constant  $k = 400$  N/m), a damper (damping constant  $c = 3$  Ns/m), and an actuator, delivering the force  $F$ . The resonance frequency of this system equals 4.5 Hz. The disturbance  $\ddot{x}_g$  [m/s<sup>2</sup>] enters at ground level. The goal of the controller design is to minimize the mass acceleration  $\ddot{x}_m$  [m/s<sup>2</sup>]. This example translates as follows to the control configuration of Fig. 1:

$$d = \ddot{x}_g; \quad (40)$$

$$x = \ddot{x}_m; \quad (41)$$

$$u = F; \quad (42)$$

$$G(s) = \frac{s^2}{ms^2 + cs + k}; \quad (43)$$

$$G_d(s) = \frac{cs + k}{ms^2 + cs + k}. \quad (44)$$

<sup>1</sup>Imposing the higher order derivatives of  $\Im(H_{11}(\omega))$  and  $\Re(H_{11}(\omega))$  to equal zero would also result in linear equality constraints in  $q_l$ .

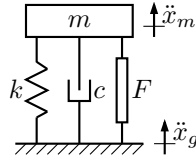


Figure 3: Simulation example: actively suspended mass.

The continuous transfer functions are discretized using the zero-order-hold discretization rule with  $f_s = 100$  Hz.  $\ddot{x}_g$  is assumed to be purely harmonic:  $M = 1$ , and  $D_1 = 0.01 \text{ m/s}^2$ . The nominal value of  $\omega_0$  equals  $9\pi \text{ rad/s}$  ( $f_0 = 4.5 \text{ Hz}$ ), and for the worst-case robust implementation a maximal uncertainty of  $1\pi \text{ rad/s}$  is considered:  $\omega_0 \in [8\pi, 10\pi] \text{ rad/s}$ .

For the optimization problem,  $N = 1000$  time samples are considered.  $Q(z)$  is parameterized by a FIR-model of length  $L = 250$ . In order to obtain results that are independent of the actuator specifications  $u_{\max}$  and  $\dot{u}_{\max}$ , the input constraints (17,18) are dropped. As a result, the non-robust optimization problem has 2255 variables, 2004 linear equality constraints, and 2000 linear inequality constraints.

In the goal function (32), the influence of the process noise is assumed to be negligible:  $\alpha_2 = 0$ . For the computation of  $f_3$ ,  $H_{13}(\omega)$  is weighted by:

$$W_{13}(\omega) = (50\pi)^2 / \omega^2. \quad (45)$$

This weighting function emphasizes the higher frequencies, and is typically used to enforce a high frequency roll-off of the loop gain [5].

To compute the trade-off curves, MINOS requires on the average 60 CPU seconds per optimization problem instance on an opteron processor.

### 3.2 Trade-off curves

Fig. 4 shows the trade-off curve for  $f_1$ , the mean square of the harmonic component of  $x(k)$ , and  $f_3$ , the weighted  $H_\infty$ -norm of  $H_{13}(\omega)$ . The trade-off curve is shown for the non-robust implementation ('nonrob'), the worst-case robust approach ('wc') and the sensitivity-based robust approach ('sens'). Note that for the worst-case approach, the abscissa corresponds to  $f_{1,wc}$  (34) instead of  $f_1$ .

By varying  $\alpha_3$  from 0 to  $\infty$ , the trade-off curve is traced from left to right. For each approach a better regulation performance for the periodic disturbance  $d(k)$  (lower  $f_1$ ) comes at the cost of a higher sensitivity to sensor noise  $n_s(k)$  (higher  $f_3$ ). The trade-off curves allow us to numerically quantify this intuitive insight. The trade-off curves do not exhibit a really pronounced 'knee'. They still suggest, however, that it is not advisable to choose  $f_1$  ( $f_{1,wc}$ ) below, say  $0.25 \cdot 10^{-3} \text{ m}^2/\text{s}^4$  since this results in a strong increase in noise sensitivity compared to the achievable reduction of  $f_1$ .

Figure 4 shows that, for a fixed value of  $f_1$ , both robust implementations always have a higher value of  $f_3$  compared to the non-robust implementation, which is of course the cost for the increased robustness. For the worst-case approach, this cost decreases monotonically as a function of  $f_{1,wc}$  and eventually vanishes. For the sensitivity-based approach, it is always nonzero and minimal around  $f_1 = 0.25 \cdot 10^{-3} \text{ m}^2/\text{s}^4$ .

The rightmost point on the trade-off curve of the non-robust and the worst-case robust approach corresponds to the open loop system<sup>2</sup>:

$$C(z) \equiv 0 \Rightarrow H_{13}(z) \equiv 0 \Rightarrow f_3 = 0, \quad (46)$$

$$\Rightarrow H_{11}(z) \equiv G_d(z). \quad (47)$$

<sup>2</sup>Note that these rightmost points in general do not coincide. This is the case for the simulation example since for the open loop system the worst case value of  $f_1$  for  $\omega_0 \in [8\pi, 10\pi] \text{ rad/s}$  is the value at  $\omega_0 = 9\pi \text{ rad/s}$ .

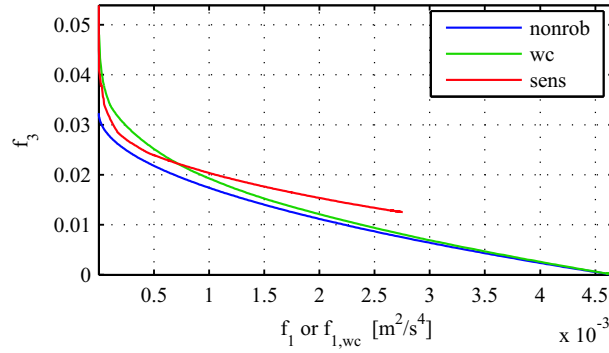


Figure 4: Trade-off curve between  $f_1$  and  $f_3$  for the non-robust implementation ('nonrob'), the worst-case robust approach ('wc') and the sensitivity-based robust approach ('sens');  $\alpha_2 = 0$ .

This can be understood as follows:  $\alpha_3 = \infty$  implies that the control engineer is only interested in reducing the sensitivity of  $x(k)$  to sensor noise as much as possible. This is achieved if  $C(z) \equiv 0$ , since in that case the sensor noise is no longer fed back to the system. However, the open loop system can only be a solution of the optimization problem if the corresponding  $\mathbf{H}(z)$  complies with all constraints. This is the case for the non-robust and the worst-case approach, but not for the sensitivity-based approach, since  $H_{11}(\omega) \equiv G_d(\omega)$  does not fulfil constraints (38,39) imposed in the latter approach. This explains why for the sensitivity-based approach the rightmost point of the trade-off curve does not correspond to  $f_3 = 0$ .

### 3.3 Evaluation of the results

This subsection evaluates the closed loop system at the intersection points of the trade-off curves with the horizontal line  $f_3 = 0.03$ .

#### 3.3.1 Performance Trade-off

Figure 5 shows the amplitude of both the sensitivity function,  $S(\omega)$ , and the complementary sensitivity function,  $T(\omega)$ . For the control system of Section 2.1 these functions are defined as [5]

$$S(\omega) \equiv \frac{1}{1 - C(\omega)G(\omega)} ; \quad (48)$$

$$T(\omega) \equiv \frac{C(\omega)G(\omega)}{1 - C(\omega)G(\omega)} . \quad (49)$$

For the control problem of Section 3.1,  $T(\omega)$  corresponds to  $H_{13}(\omega)$ . By using weighting function (45) for the weighted  $H_\infty$ -norm of  $H_{13}(\omega)$ , a second-order roll-off of  $T(\omega)$  at high frequencies is obtained.

Looking at the sensitivity function, good attenuation of the periodic disturbance corresponds to a low value of  $|S|$  at  $\omega_0 = 9\pi$  rad/s (in Fig. 5  $\omega_0$  is indicated by the vertical dotted line).  $S(\omega)$  peaks at low frequencies since at these frequencies no restrictions are imposed on  $S(\omega)$ . Since the following property applies to  $S(\omega)$  and  $T(\omega)$ , [5]:

$$||S(\omega)| - |T(\omega)|| \leq 1 , \quad (50)$$

$T(\omega)$  also has a high amplitude at low frequencies. This undesired low-frequency behavior can be prevented by considering low frequency process noise, by including the weighted  $H_\infty$ -norm of  $S(\omega)$  in the goal function, or by changing  $W_{13}(\omega)$  appropriately.

The trade-off between  $f_1$ , the regulation of the periodic disturbance, and  $f_3$ , the attenuation of the sensor noise translates as follows to  $S(\omega)$  and  $T(\omega)$ : Minimizing  $f_3$  aims at reducing the bandwidth, the frequency

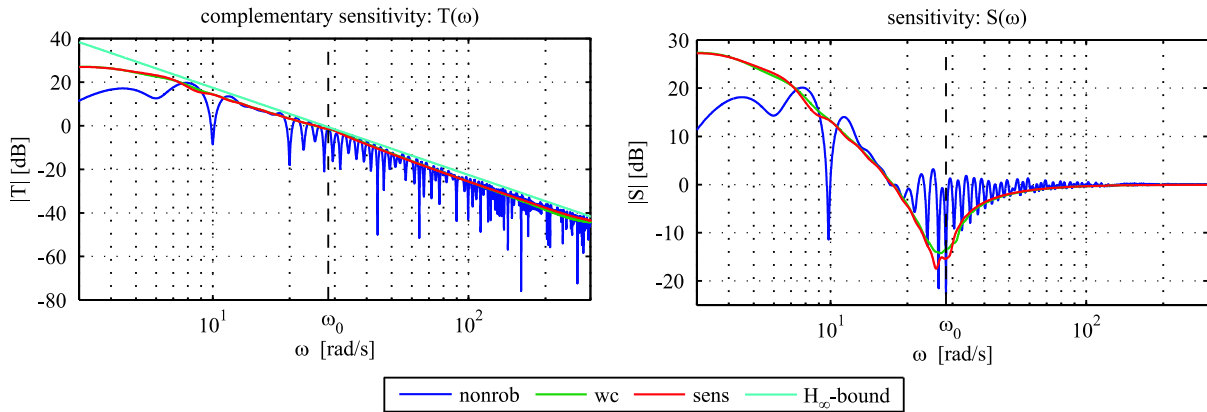


Figure 5: Amplitude of the complementary sensitivity function  $T(\omega)$  and the sensitivity function  $S(\omega)$  for the non-robust implementation ('nonrob'), the worst-case robust approach ('wc') and the sensitivity-based robust approach ('sens');  $f_3 = 0.03$ .

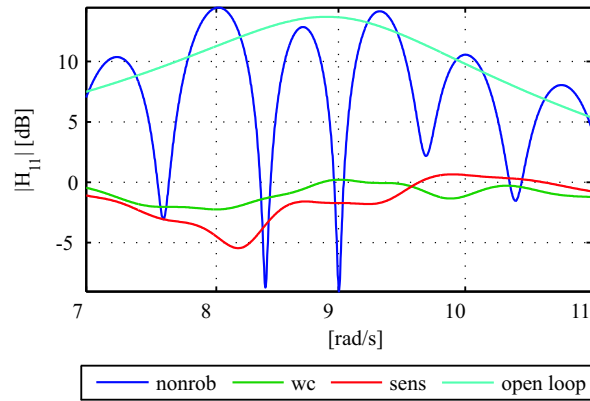


Figure 6: Amplitude of  $H_{11}(\omega)$  for the non-robust implementation ('nonrob'), the worst-case robust approach ('wc'), the sensitivity-based robust approach ('sens') and the open loop system ('open loop');  $f_3 = 0.03$ .

at which  $T(\omega)$  crosses the -3dB line, of the closed-loop system as much as possible. Whenever a sufficiently high weight on  $f_1$  is imposed, the sensitivity function prevents the bandwidth from dropping below  $9\pi$  rad/s, since at this point  $|S| \simeq 0$  and consequently,  $|T| \simeq 1$ .

### 3.3.2 Robustness Analysis

Figure 6 shows the amplitude of  $H_{11}(\omega)$  for  $\omega$  close to  $9\pi$  rad/s, the nominal value of  $\omega_0$ . Since in the simulation example  $d(k)$  contains only one harmonic, robustness of the solution for uncertainty on  $\omega_0$  is readily assessed from the amplitude plot of  $H_{11}(\omega)$  near  $\omega_0 = 9\pi$  rad/s. Robust solutions are characterized by a low amplitude not only for  $\omega_0 = 9\pi$  rad/s, but also for the nearby frequencies.

At  $9\pi$  rad/s the non-robust approach has the largest attenuation of the disturbance, but the solution is clearly not robust for uncertainty on  $\omega_0$ . Within an uncertainty range of 1 rad/s, the periodic disturbance may even be amplified. Both the robust approaches yield less attenuation at  $\omega_0 = 9\pi$  rad/s, but for small deviations in  $f_0$ , they still provide a good attenuation of  $d(k)$ .

Remark that in order to obtain a finite dimensional optimization problem, the framework imposes a discretization of the frequency axis. This may lead to an underestimation of both the weighted  $H_\infty$  norms of

$H_{12}(z)$  (14) and  $H_{13}(z)$  (14) and the worst-case goal function  $f_{1,wc}$  (34). For the simulation example  $\delta f$  equals 0.1 Hz. In Fig. 5 and 6, a higher frequency resolution of 0.001 Hz is used in order to show that for this application the discretization causes no problems.

## 4 Conclusion

A general framework is developed for the design of optimal regulators for periodic disturbances with known frequency content. Compared to classical  $H_\infty$ -synthesis the proposed framework has the following advantages: First, it naturally allows focussing on disturbance rejection at discrete frequency *lines*.  $H_\infty$ -synthesis, on the other hand, is naturally suited to impose vibration suppression in a frequency *range*, which is too strict a constraint in the case of disturbances with few harmonics, and therefore might result in a loss of performance. Numerically quantifying this performance loss is the subject of future work. Second, input constraints such as bound and rate constraints on the control signal are readily implemented in the framework, while this implementation is more cumbersome in  $H_\infty$ -control. Third, the framework allows for the computation of trade-off curves for competing performance specifications which is not straightforward in  $H_\infty$ -control.

Future research will address the applicability of the framework to other kinds of disturbances like impact disturbances. It will also be investigated how the robustness strategies adopted in this paper extend to other kinds of uncertainties, like uncertainty on the frequency content,  $D_m$ , of  $d(k)$  or parametric plant uncertainties.

## Acknowledgements

Goele Pipeleers is a research assistant of the Fund for Scientific Research (FWO) - Flanders (Belgium). Bram Demeulenaere is a postdoctoral fellow of the Fund for Scientific Research (FWO) - Flanders (Belgium). The support of K.U.Leuven-BOF EF/05/006 Center-of-Excellence Optimization in Engineering is gratefully acknowledged.

## References

- [1] S. Boyd, C. Barratt, *Linear Controller Design: Limits of Performance*, Prentice-Hall, Englewood Cliffs (1991).
- [2] S. Boyd, L. Vandenberghe, *Convex Optimization*, Cambridge University Press (2004).
- [3] B. A. Murtagh, M. A. Saunders, *MINOS 5.5 User's Guide* (1998).
- [4] G. Pinte, R. Boonen, P. Sas, W. Desmet, *Active control of impact noise of punching machines*, in *Proceedings of the Twelfth International Congress on Sound and Vibration*, Portugal (2005).
- [5] S. Skogestad, I. Postletwaite, *Multivariable Feedback Control: Analysis and Design*, John Wiley & Sons (2005).

